

ARTICLE OPEN



XBP1 modulates endoplasmic reticulum and mitochondria crosstalk via regulating NLRP3 in renal ischemia/reperfusion injury

Haiqiang Ni^{1,5}, Zhiyu Ou^{1,5}, Yuchen Wang^{1,5}, Yanna Liu^{2,5}, Kailun Sun^{3,4}, Ji Zhang^{3,4}, Jiasi Zhang^{3,4}, Wenfeng Deng¹, Wenli Zeng¹, Renfei Xia¹, Jian Xu¹, Nianqiao Gong^{1,3,4} and Yun Miao¹

© The Author(s) 2023

The functional status of mitochondria and the endoplasmic reticulum are central to renal ischemia/reperfusion injury (IRI). X-box binding protein 1 (XBP1) is an important transcription factor in endoplasmic reticulum stress. NLR family pyrin domain containing-3 (NLRP3) inflammatory bodies are closely related to renal IRI. In vivo and in vitro, we examined the molecular mechanisms and functions of XBP1-NLRP3 signaling in renal IRI, which influences ER-mitochondrial crosstalk. In this study, mice were subjected to 45 min of unilateral renal warm ischemia, the other kidney resected, and reperfusion was performed for 24 h in vivo. In vitro, murine renal tubular epithelial cells (TCMK-1) were exposed to hypoxia for 24 h and reoxygenation for 2 h. Tissue or cell damage was evaluated by measuring blood urea nitrogen and creatinine levels, histological staining, flow cytometry, terminal deoxynucleotidyl transferase-mediated nick-end labeling, diethylene glycol staining, and transmission electron microscopy (TEM). Western blotting, immunofluorescence staining, and ELISA were used to analyze protein expression. Whether XBP1 regulates the NLRP3 promoter was evaluated using a luciferase reporter assay. Kidney damage was reduced with decreasing blood urea nitrogen, creatinine, interleukin-1 β , and interleukin-18 levels. XBP1 deficiency reduced tissue damage and cell apoptosis, protecting the mitochondria. Disruption of XBP1 was associated with reduced NLRP3 and cleaved caspase-1 levels and markedly improved survival. In vitro in TCMK-1 cells, XBP1 interference inhibited caspase-1-dependent mitochondrial damage and reduced the production of mitochondrial reactive oxygen species. The luciferase assay showed that spliced XBP1 isoforms enhanced the activity of the NLRP3 promoter. These findings reveal that XBP1 downregulation suppresses the expression of NLRP3, a potential regulator of endoplasmic reticulum mitochondrial crosstalk in nephritic injury and a potential therapeutic target in XBP1-mediated aseptic nephritis.

Cell Death Discovery (2023)9:69; <https://doi.org/10.1038/s41420-023-01360-x>

INTRODUCTION

Acute kidney injury (AKI) is associated with severe morbidity and mortality and is prevalent globally. However, the mechanisms underlying renal dysfunction and tissue damage remain to be fully elucidated [1]. Ischemia/reperfusion, a common cause of AKI [2], involves inflammation, hemodynamic alterations, and epithelial and endothelial cell death [3, 4]. Accumulating evidence reveals that ischemia/reperfusion injury (IRI) is a multifactorial process in which the mitochondria and endoplasmic reticulum (ER) play central roles [5]. Recent studies have shown that injury to the ER or mitochondria could disrupt ER-mitochondrial crosstalk in the kidneys, leading to renal injury. Thus, ER-mitochondria crosstalk may be a potential therapeutic target in AKI [6].

A dysfunctional ER may contribute to the accumulation of unfolded or misfolded proteins during IRI, causing ER stress (ERS). Upon the detection of unfolded proteins, three transmembrane receptors in the ER, namely ATF6, IRE1 α , and PERK, activate the

unfolded protein response signaling pathway [7–9]. Low levels of the unfolded protein response protect the kidneys from renal IRI [10]. However, severe ERS induces the activation of cell death cascades [11, 12]. ERS leads to the opening of the mitochondrial permeability transition pore (mPTP), which then depletes the mitochondrial membrane potential (MMP) and triggers the release of mitochondrial pro-apoptotic signals [13], reduction in MMP, and release of cytochrome c (Cyt-c) and other apoptosis-related factors. In particular, AKI-induced mitochondrial reactive oxygen species (mROS) promote the activation of the NLRP3 inflammasome, leading to caspase 1-dependent production of gasdermin D (GSDMD)-mediated pyroptosis and the maturation of the pro-inflammatory cytokines interleukin (IL)-1 β and IL-18 [14–16].

Recent studies have examined the regulatory functions of the mitochondria-associated ER membranes (MAMs). Aside from ER chaperones, other inflammatory factors such as sigma-1 receptor [17], IP (3) receptor [18], GRP78 [19], calnexin [20], IRE1 α , and PERK

¹Department of Transplantation, Nanfang Hospital, Southern Medical University, 510515 Guangzhou, China. ²Department of Gastroenterology and Hepatology, Beijing Youan Hospital, Capital Medical University, 100069 Beijing, China. ³Institute of Organ Transplantation, Tongji Hospital, Tongji Medical College, Huazhong University of Science and Technology, 430030 Wuhan, China. ⁴Key Laboratory of Organ Transplantation of Ministry of Education, National Health Commission and Chinese Academy of Medical Sciences, 430030 Wuhan, China. ⁵These authors contributed equally: Haiqiang Ni, Zhiyu Ou, Yuchen Wang, Yanna Liu. [✉]email: nqgong@tjh.tjmu.edu.cn; miaoyunecho@126.com

Received: 24 June 2022 Revised: 1 February 2023 Accepted: 2 February 2023

Published online: 17 February 2023

can also modulate ER-mitochondrial crosstalk [21–23]. When the mitochondrial fission protein, fission 1 homolog (Fis1), binds to B cell receptor-associated protein 31 (BAP31) located in the MAMs and forms the Fis1-BAP31 complex, cell death signals are conveyed to the ER lumen, initiating the cell apoptosis pathway [24]. Under ERS, unspliced X-box-binding protein 1 (XBP1u) mRNA (a non-transcriptional form) is activated by the RNase activity of IRE1 α , which excises 26 nucleotides, causing a frameshift and forming a transcriptionally spliced XBP1 (XBP1s) mRNA [25]. The transcription factor XBP1s then regulates a series of important target genes to determine cell fate [26]. XBP1 downregulation has been found to reduce renal IRI by inhibiting HRD1-mediated NRF2 ubiquitination [27]. Although XBP1 downregulation under severe stress is known to protect tissues and organs, how (or even whether) XBP1 participates in the ER-mediated regulation of mitochondria or MAMs in renal IRI remains unknown. To address this, we examined how the XBP1-NLRP3 axis modulates ER-mitochondrial crosstalk during renal IRI in vivo and in vitro.

RESULTS

IRI triggers severe ERS and markedly increases XBP1s expression

To detect ER morphology in IRI kidney sections, ultrastructural analysis was performed using TEM. Abnormal ER morphology, manifested as distinct vacuolation and swelling (characteristic of ERS), was observed (Fig. 1A). To further evaluate ERS, western blotting was used to analyze the expression of key ERS markers in the BIP and IRE1 α pathway (IRE1 α , XBP1u, XBP1s, and p-ASK1), PERK pathway (PERK, p-PERK, CHOP, ATF4, and NRF2), and the ATF6 pathway. The fold-changes in expression relative to the control were 1.24 ± 0.08 ($P < 0.05$) for BIP, 3.14 ± 0.73 ($P < 0.05$) for IRE1 α , 2.25 ± 0.29 ($P < 0.05$) for XBP1u, 6.04 ± 1.36 , ($P < 0.05$) for XBP1s, 2.53 ± 0.12 ($P < 0.001$) for p-ASK1, 1.04 ± 0.01 ($P < 0.05$) for PERK, 5.31 ± 0.57 ($P < 0.01$) for p-PERK, 4.29 ± 1.03 ($P < 0.05$) for CHOP, 2.69 ± 0.60 ($P < 0.05$) for ATF4, 3.89 ± 0.90 ($P < 0.05$) for NRF2, and 5.11 ± 1.00 ($P < 0.05$) for ATF6. Notably, the fold-change was significantly greater for XBP1s than for the other proteins, indicating that this activated transcription factor may play a key role in response to IR-induced kidney injury.

IRI induces mitochondrial injury and NLRP3 inflammasome activation

Mitochondrial damage and the NLRP3 inflammasome play important roles in ischemia-reperfusion injury [27–29]. TEM confirmed mitochondrial damage, characterized by mitochondrial swelling, cristae fracture, membrane damage, and abnormal ER in the vicinity of the MAMs (Fig. 2A). The relative expressions of the mitochondrial damage markers total Cyt-c and caspase-9 (Casp9) were significantly elevated relative to the control (Cyt-c: 0.56 ± 0.04 vs. 0.84 ± 0.08 , $P < 0.05$; Casp9, p39: 0.06 ± 0.01 vs. 0.83 ± 0.12 , $P < 0.01$; Casp9, p37: 0.12 ± 0.02 vs. 2.53 ± 0.33 , $P < 0.01$; Fig. 2B). Western blot analysis revealed a significantly elevated expression of NLRP3 molecules and caspase-1 activators in the IRI group relative to the control (0.10 ± 0.01 vs. 0.14 ± 0.01 and 1.02 ± 0.12 vs. 1.50 ± 0.03 , respectively, $P < 0.01$; Fig. 2C), indicating inflammasome activation. In addition, immunoelectron microscopy (IEM) revealed an enhanced NLRP3 colocalization with mitochondria under IRI, and that NLRP3 may even be able to translocate to the MAMs (Fig. 2D).

The molecular mechanism of the crosstalk between ERS and mitochondrial dysfunction in response to IRI is mediated by the XBP1-NLRP3 axis

To further analyze the effect of XBP1 modulation on NLRP3 expression and activity, we transfected TCMK-1 cells with an XBP1-overexpression lentivirus. In these cells, the relative RNA expression of XBP1u was 1.21 ± 0.11 vs. 3.25 ± 0.48 , and that of XBP1s

was 0.82 ± 0.41 vs. 19.49 ± 5.41 . Meanwhile, the protein expression of XBP1u was 0.47 ± 0.06 vs. 0.74 ± 0.06 , and that of XBP1s was 0.20 ± 0.04 vs. 0.45 ± 0.06 (all $P < 0.05$). Further, increased XBP1 expression enhanced NLRP3 expression (mRNA, 1.01 ± 0.01 vs. 1.18 ± 0.04 ; protein, 0.37 ± 0.06 vs. 0.72 ± 0.10 ; both $P < 0.05$). For TCMK-1 cells transfected with XBP1-targeting siRNA, the values relative RNA expression levels were as follows: for XBP1u, 0.84 ± 0.03 vs. 0.03 ± 0.01 , $P < 0.01$; for XBP1s, 1.19 ± 0.09 vs. 0.02 ± 0.01 , $P < 0.001$. The relative protein expression values were 0.48 ± 0.05 vs. 0.05 ± 0.01 , $P < 0.001$ for XBP1u and 0.17 ± 0.03 vs. 0.03 ± 0.01 , $P < 0.05$ for XBP1s. Relative to the empty-vector group, NLRP3 expression was lower in the si-XBP1 group (mRNA: 1.02 ± 0.01 vs. 0.54 ± 0.04 , $P < 0.001$; protein: 0.40 ± 0.07 vs. 0.10 ± 0.01 , $P < 0.05$) (Fig. 3A, B). Moreover, XBP1s production was inhibited upon treatment with 4 μ 8c, an IRE1 α inhibitor, further reducing NLRP3 expression (Supplementary Fig. S1).

To further verify the effects of XBP1 on NLRP3 under stress conditions, H/R was used to simulate renal IRI in vitro. Our experiments revealed that XBP1 downregulation inhibited NLRP3 expression (XBP1u: 1.24 ± 0.15 vs. 0.34 ± 0.13 , $P < 0.05$; XBP1s: 0.27 ± 0.03 vs. 0.03 ± 0.01 , $P < 0.01$; NLRP3: 0.97 ± 0.07 vs. 0.22 ± 0.02 , $P < 0.001$; Fig. 3C).

We then examined the mechanisms through which XBP1 regulates NLRP3. Based on bioinformatics analysis, we predicted that XBP1 might regulate NLRP3 promoter activity via XBP1s. We conducted a dual-luciferase reporter assay to confirm if XBP1s binds to the NLRP3 promoter. First, we constructed an XBP1s-overexpression plasmid containing the NLRP3 promoter. This, along with a luciferase reporter plasmid, was transfected into 293T cells. Before interaction with the XBP1s transcription factor, NLRP3 promoter activity was 13.52 times higher in the XBP1-overexpression group than in the control group ($P < 0.05$), indicating activation of the NLRP3 gene promoter. After interacting with the XBP1s transcription factor, NLRP3 gene promoter activity was 1.81 times higher than in the control group, indicating that the XBP1s transcription factor enhances NLRP3 gene promoter activity ($P < 0.05$; Fig. 3D). Unfortunately, we obtained negative results for our three predicted binding sites. Therefore, the binding sites require further investigation.

XBP1 downregulation reduced the production of NLRP3 downstream effectors, mitochondrial damage, and apoptosis in TCMK-1 cells exposed to H/R

After elucidating the possible mechanism whereby XBP1 regulates NLRP3, we examined whether XBP1 downregulation affects the expression of the downstream effector molecules of NLRP3 in vitro. We then verified the changes in NLRP3 localization following XBP1 downregulation using a mitochondrial probe (MitoTracker), ER probe (ER Tracker Blue White DPX dye), and anti-NLRP3 antibodies and observed them via confocal microscopy. Under hypoxia, colocalization with NLRP3 was enhanced in the mitochondria and ER; colocalization at all three sites was reduced after XBP1 downregulation (Fig. 4A). Based on western blot analysis, XBP1 downregulation inhibited inflammation in TCMK-1 cells after 24 h of hypoxia followed by 2 h of reoxygenation, which was not exhibited in the siRNA-treated control (Casp1, p20: 1.31 ± 0.10 vs. 0.10 ± 0.01 , $P < 0.01$; IL-1 β : 0.99 ± 0.10 vs. 0.26 ± 0.07 , $P < 0.05$; IL-18: 0.54 ± 0.06 vs. 0.16 ± 0.03 , $P < 0.05$; Fig. 4B).

We then examined the protective effect of XBP1 inhibition on the mitochondria using an in vitro H/R model. To do this, we used a DCFH-DA probe to stain the total reactive oxygen species (tROS) and the mitochondrial superoxide indicator MitoSOX red to stain mitochondrial ROS (mROS). ROS were detected via flow cytometry. MMP was detected via staining with the fluorescent dye JC-1, followed by flow cytometry. The results showed that siRNA-induced XBP1 downregulation reduced ROS production (tROS: 221 ± 20.11 vs. 97.60 ± 8.17 , $P < 0.01$; mROS: 56.27 ± 2.21 vs. 43.77 ± 0.98 , $P < 0.01$; Fig. 4C), and elevated the MMP

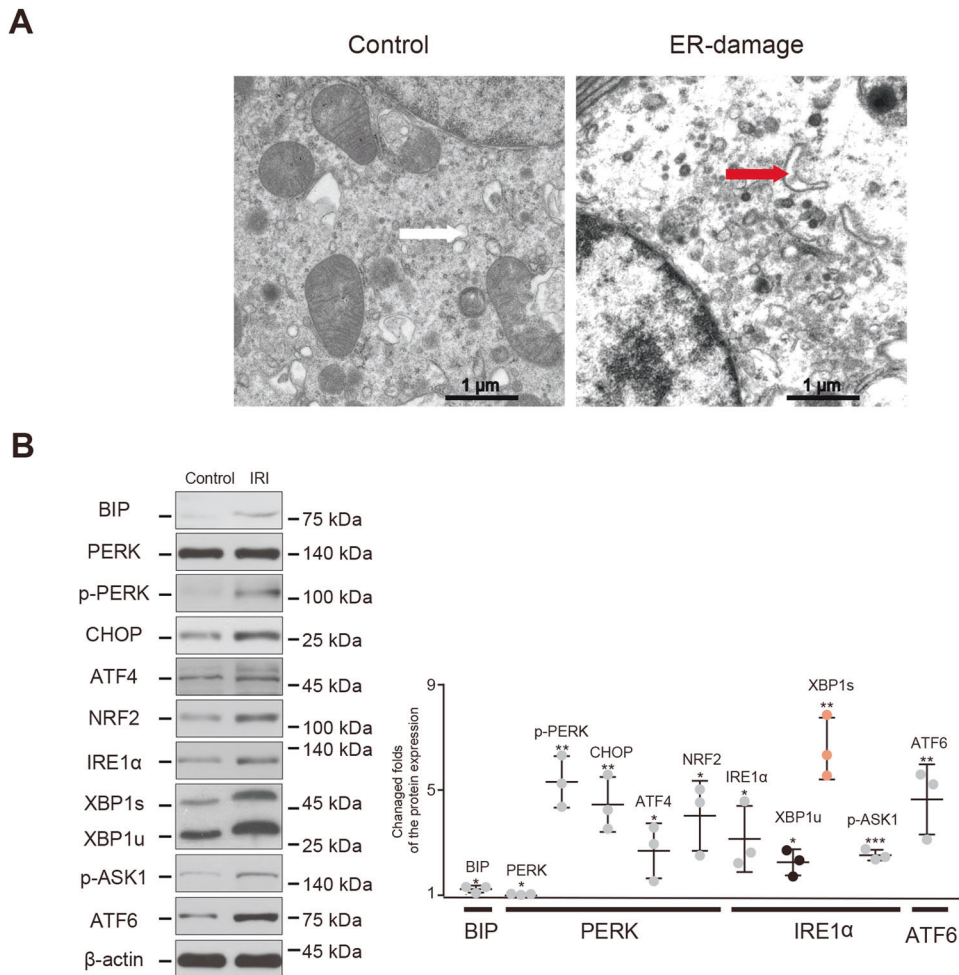


Fig. 1 IRI triggers severe ERS and noticeable XBP1s expression. To construct the mouse IRI model, we used microvascular clips to block the left renal pedicle of the mouse for 45 min and cut off the right kidney after opening the bloodstream. **A** TEM analysis showed ER damage was induced by IRI. The white arrow indicates the normal ER, while the red arrow indicates swollen ER lumens. Scale bar = 1 μ m; \times 5000 magnification. **B** The expression levels of ER stress markers were detected using western blotting. The protein level of XBP1s was considerably higher than that of other molecules after IRI, as shown by the fold-changes. $*P < 0.05$, $**P < 0.01$, $***P < 0.001$ vs. The normal control group ($n = 3$ samples/group). IRI ischemia/reperfusion injury, ER endoplasmic reticulum.

(72.77 ± 0.91 vs. 45.53 ± 1.29 , $P < 0.0001$; Fig. 4D). These changes did not occur in the si-negative control (NC)-transfected cells. These results indicate that XBP1 inhibition can protect mitochondrial function in an in vitro H/R cell model.

Western blot analysis of Cyt-c and Casp9 expression revealed that the rates of mitochondrial damage were lower in the si-XBP1-treated group than in the control (Casp9, p39: 1.38 ± 0.07 vs. 0.09 ± 0.01 , $P < 0.05$; Casp9, p37: 0.65 ± 0.19 vs. 0.05 ± 0.02 , $P < 0.0001$; Cyt-c: 1.03 ± 0.14 vs. 0.30 ± 0.08 , $P < 0.05$; Fig. 4E).

To detect apoptosis, we conducted Annexin V/PI analysis (22.01 ± 1.56 vs. 17.03 ± 0.36 , $P < 0.05$; Fig. 4F) and used western blotting to measure the expression of caspase-3 (Casp3), a key apoptosis marker (Casp3, p19: 0.59 ± 0.14 vs. 0.16 ± 0.07 , $P < 0.05$; Casp3, p17: 2.15 ± 0.04 vs. 1.33 ± 0.22 , $P < 0.05$; Fig. 4G). The proportion of apoptotic cells was lower in the si-XBP1 group than in the control group.

Genotyping of Xbp1^{+/-} mice

The heterozygous murine Xbp1^{+/-} allele contains a trapping cassette, the splice acceptor- β -geo-polyA (SA- β geo-pA), which is flanked by the flippase recombination target of the upstream exon. This causes the truncation of endogenous transcripts and constitutive null mutations that reduce XBP1 expression (Fig. 5A).

Genotyping of Xbp1^{+/-} mice was confirmed via PCR using Ef and Kr primers (Fig. 5B).

Downregulation of XBP1-NLRP3 signaling reduced the crosstalk between ERS and mitochondrial damage and protected the kidneys of Xbp1^{+/-} mice from IRI

To evaluate the importance of the XBP1-NLRP3 axis in the crosstalk between ERS and mitochondrial damage in IR-induced renal inflammation, we studied heterozygous Xbp1^{+/-} mice generated using the knockout-first strategy. XBP1 expression was observed to be somewhat lower in the kidneys of Xbp1^{+/-} mice subjected to ischemia-reperfusion than in the control group, resulting in reduced NLRP3 expression (XBP1u: 1.09 ± 0.039 vs. 0.70 ± 0.04 , $P < 0.01$; XBP1s: 0.29 ± 0.01 vs. 0.14 ± 0.01 , $P < 0.001$; NLRP3: 0.14 ± 0.01 vs. 0.05 ± 0.01 , $P < 0.01$; Fig. 6A). IEM revealed the reduced localization of NLRP3 in the mitochondria or MAMs of Xbp1^{+/-} mice. TEM revealed that the Xbp1^{+/-} mice had more complete mitochondrial structures than the control mice (Fig. 6B). In Xbp1^{+/-} mice, following mitochondrial damage, there was lower production of ROS (76.07 ± 3.19 vs. 36.88 ± 1.60 ; $P < 0.001$) and Cyt-c (0.84 ± 0.08 vs. 0.26 ± 0.03 ; $P < 0.01$), and caspase-9 activation was inhibited (Casp9, p39: 0.83 ± 0.12 vs. 0.16 ± 0.01 , $P < 0.01$; Casp9, p37: 2.53 ± 0.33 vs. 0.40 ± 0.07 , $P < 0.01$) (Fig. 6C, D). Xbp1^{+/-} mice also exhibited a reduced expression of

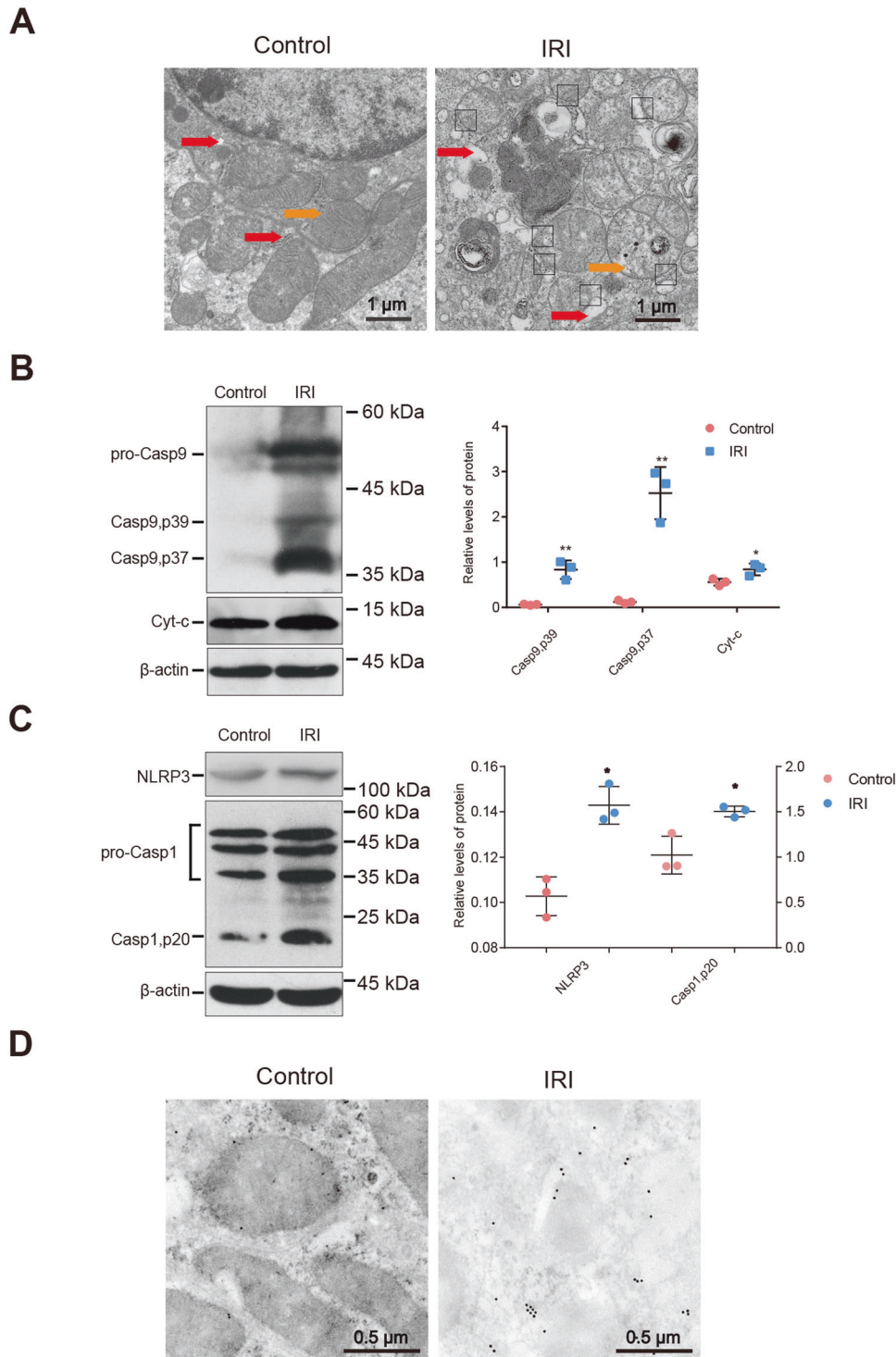


Fig. 2 IRI induces mitochondrial injury and NLRP3 inflammasome activation. To construct the mouse IRI model, we used microvascular clips to block the left renal pedicle of the mouse for 45 min and then cut off the right kidney after opening the bloodstream. **A** ERS and mitochondrial damage developed simultaneously. TEM analysis showed that the ER maintained an appropriate distance or formed a direct connection with the mitochondria. The white arrow indicates normal ER, the black arrow indicates normal mitochondria, the red arrow indicates ER swelling, the orange arrow indicates damaged mitochondria, and the blank rectangle indicates MAMs. Scale bar = 1 μ m; $\times 5000$ magnification. **B** The protein expression of caspase-9 and total Cyt-c were increased in the IRI group. Western blot; $*P < 0.05$, $**P < 0.01$ vs. the normal control group ($n = 3$ samples/group). **C** The expressions of NLRP3 and caspase-1 were increased in the IRI group. Western blot; $*P < 0.05$ vs. the normal control group ($n = 3$ samples/group). **D** IEM analysis showed more NLRP3 translocated to the mitochondria or MAMs after renal IRI. The red arrow indicates the ER, the orange arrow indicates the mitochondria, the blank rectangle indicates the MAMs, and the small black dots indicate 10-nm colloidal gold particles. Scale bar = 0.5 μ m; $\times 10,000$ magnification. IRI ischemia/reperfusion injury, ER endoplasmic reticulum, MAMs mitochondria-associated endoplasmic reticulum membranes.

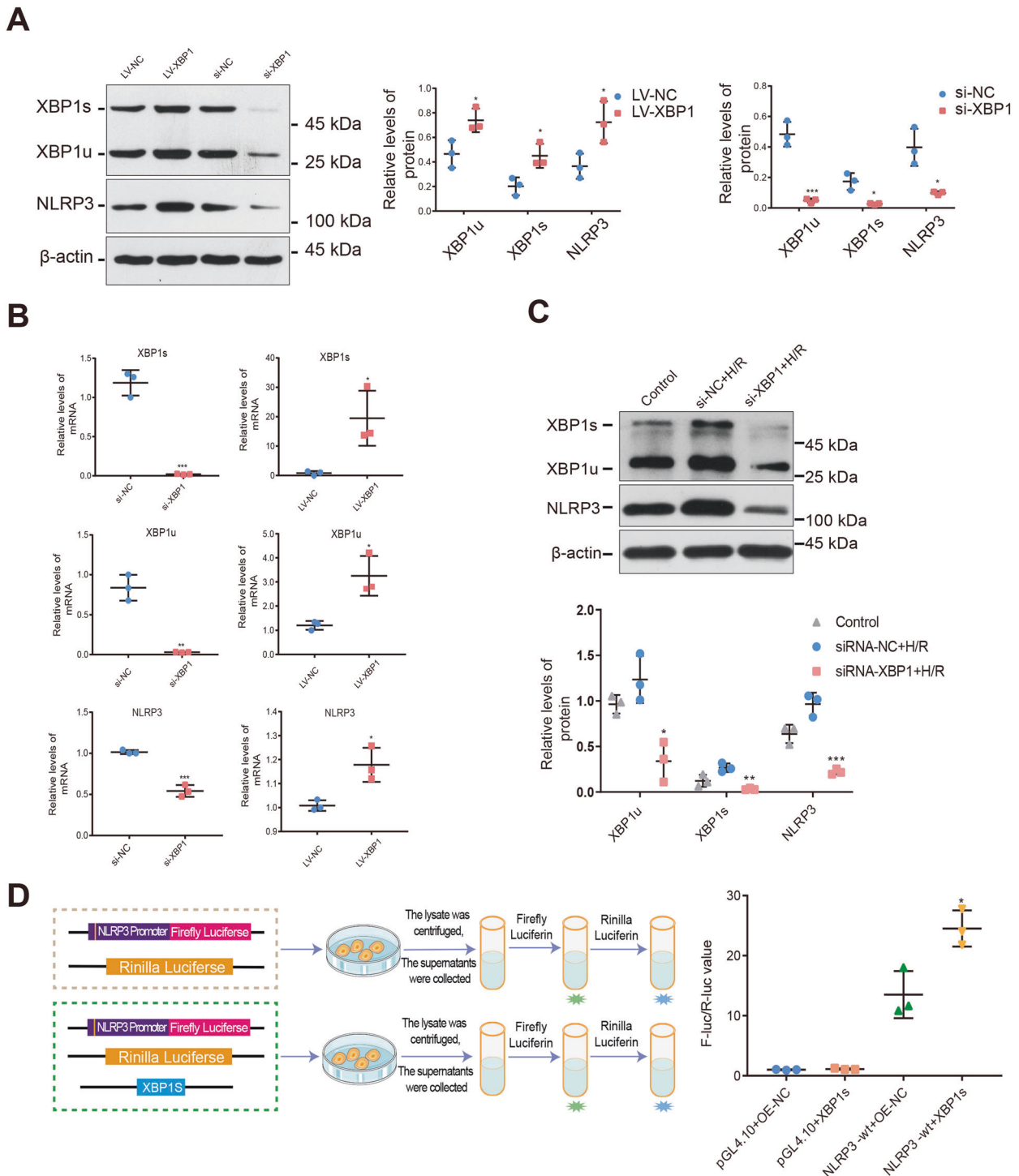
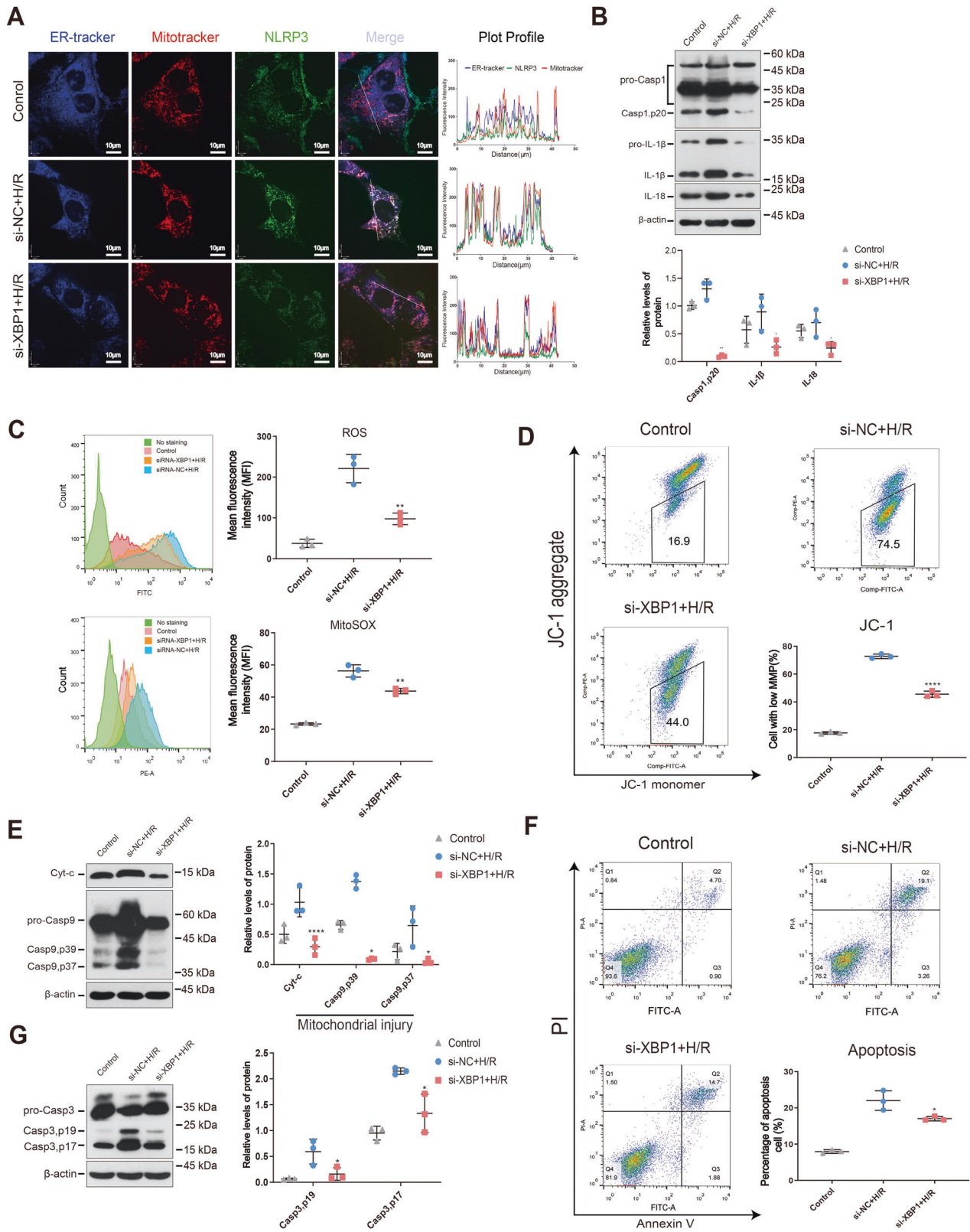


Fig. 3 The XBP1-NLRP3 axis forms a molecular mechanism involved in the crosstalk between ERS and mitochondrial dysfunction in response to IRI. TCMK-1 cells were transfected with lenti-*Xbp1*, siRNA-*Xbp1*, and corresponding control vectors, respectively. For the cell H/R model, hypoxia was performed in a tri-gas hypoxia incubator for 24 h, and then reoxygenation was performed for 2 h after applying a fresh medium. **A** NLRP3 protein expression correlated with XBP1 protein expression following lenti-*Xbp1* and siRNA-*Xbp1* transfection. Western blot; * $P < 0.05$, *** $P < 0.001$ vs. the normal control group ($n = 3$ samples/group). **B** NLRP3 mRNA expression correlated with XBP1 mRNA expression following lenti-*Xbp1* and siRNA-*Xbp1* transfection. Real-time quantitative reverse-transcription PCR; * $P < 0.05$, ** $P < 0.01$, *** $P < 0.001$ vs. normal control group ($n = 3$ samples/group). **C** TCMK-1 cells were transfected with siRNA-*Xbp1* or siRNA-control before H/R. NLRP3 protein expression correlated with XBP1 protein expression after H/R, as shown in the western blot and densitometric analysis. * $P < 0.05$, ** $P < 0.01$, *** $P < 0.001$ vs. the normal control H/R group. **D** The pGL4.10 firefly luciferase reporter plasmids with the wild-type (WT) NLRP3 promoter were transiently transfected into 293T cells together with the pcDNA3.1(+)-XBP1s plasmid or overexpression (OE) negative control and a Renilla luciferase reporter for normalization. Luciferase activities were measured after 48 h. The results showed that the NLRP3 promoter activity of the XBP1 overexpression group was higher than that of the control group; * $P < 0.05$. Further details are shown in the “Materials and methods” section. LV-NC lentivirus normal control, si-NC siRNA normal control, H/R hypoxia/reoxygenation.



caspase-3 (Casp3, p19: 0.76 ± 0.14 vs. 0.13 ± 0.02 , $P < 0.05$; Casp3, p17: 0.47 ± 0.06 vs. 0.07 ± 0.02 , $P < 0.01$) and caspase-1 (1.50 ± 0.03 vs. 0.24 ± 0.16 , $P < 0.01$). These results reveal that inhibiting NLRP3 expression reduced NLRP3-induced apoptosis and inflammasome activation (Fig. 6E).

We then performed ELISA to examine the expression of IL-1 β (915.50 ± 41.19 vs. 31.57 ± 7.33 , $P < 0.0001$) and IL-18 (723.90 ± 27.08 vs. 303.60 ± 34.05 , $P < 0.001$) in the mouse serum (Fig. 6F). These findings indicate that the NLRP3-inflammasome-induced inflammatory response was greatly attenuated in Xbp1^{+/-} mice.

Fig. 4 Downregulation of XBP1 ameliorated NLRP3 downstream molecules, mitochondrial damage, and apoptosis in TCMK-1 cells exposed to H/R. TCMK-1 cells were transfected with lenti-*Xbp1*, siRNA-*Xbp1*, and their corresponding control vectors. For the cell H/R model, hypoxia was induced in a tri-gas hypoxia incubator for 24 h, and then reoxygenation was performed for 2 h after adding fresh culture medium. **A** Colocalization of the ER, mitochondria, and NLRP3 after siRNA-*Xbp1* transfection in TCMK-1 cells exposed to H/R as analyzed using confocal microscopy. Plot profile: the histograms (right panels) represent densities along the white bars: blue = ERtracker, red = Mitotracker, green = NLRP3, purple = overlap of ERtracker and Mitotracker, yellow = overlap of NLRP3 and Mitotracker, cyan = overlap of NLRP3 and ERtracker. Scale bar = 10 μ m. Original magnification of photograph: $\times 1000$. **B** Silencing of XBP1 led to the inhibition of inflammation (caspase-1, IL-1 β , and IL-18) in TCMK-1 cells exposed to H/R. Western blot; * $P < 0.05$, ** $P < 0.01$ vs. the siRNA-control H/R group ($n = 3$ samples/group). **C** H/R-induced ROS (tROS and mROS) production was significantly attenuated in TCMK-1 cells treated with *Xbp1* siRNA, as shown using flow cytometry. ** $P < 0.01$ vs. the siRNA-control H/R group ($n = 3$ samples/group). **D** Treatment with *Xbp1* siRNA dramatically increased the mitochondrial membrane potential in TCMK-1 cells exposed to H/R, as shown using flow cytometry. * $P < 0.05$ vs. the siRNA-control H/R group ($n = 3$ samples/group). **E** Total Cyt-c and cleaved caspase-9 expression were reduced by siRNA-*Xbp1* transfection in H/R-exposed TCMK-1 cells. Western blot; * $P < 0.05$, **** $P < 0.0001$ vs. the siRNA-control H/R group ($n = 3$ samples/group). **F** The apoptotic proportion of H/R-exposed TCMK-1 cells was decreased by siRNA-*Xbp1* transduction, as revealed using flow cytometry. * $P < 0.05$ vs. the siRNA-control H/R group ($n = 3$ samples/group). **G** Cleaved caspase-3 (p17 and p19) expression was decreased by siRNA-*Xbp1* transfection in TCMK-1 cells exposed to H/R. Western blot; * $P < 0.05$ vs. the siRNA-control H/R group ($n = 3$ samples/group). si-NC siRNA normal control, H/R hypoxia/reoxygenation.

TUNEL staining revealed renal cell apoptosis was reduced in *Xbp1*^{+/-} mice (10.65 ± 0.53 vs. 3.10 ± 0.24 , $P < 0.001$; Fig. 6G). Compared with the control, XBP1 inhibition in *Xbp1*^{+/-} mice reduced IR-induced kidney damage and histological scores (0.95 ± 0.21 vs. 3.75 ± 0.35 , $P < 0.01$, Fig. 6H), and serum creatinine (191.70 ± 5.04 vs. 97.33 ± 10.17 , $P < 0.01$) and blood urea nitrogen levels (68.27 ± 0.64 vs. 47.86 ± 0.64 , $P < 0.0001$) (Fig. 6I).

The 14-day survival analysis revealed that *Xbp1*^{+/-} mice displayed significantly longer survival than wild-type mice that received the same treatment ($P < 0.001$, Fig. 6J).

DISCUSSION

In this study, we examined how the XBP1-NLRP3 axis modulates ER-mitochondrial crosstalk during renal IRI in vivo and in vitro. To the best of our knowledge, this is the first study to examine the pivotal role of the XBP1-NLRP3 signaling pathway in regulating NLRP3-mediated cell injury in renal IRI. XBP1 increased the expression of the NLRP3 promoter and enhanced its transcriptional activity, which is necessary to induce renal injury. XBP1 knockdown inhibited NLRP3-mediated inflammation, thus regulating the interaction between the mitochondria and MAMs, thereby reducing apoptosis activation and alleviating IRI-induced AKI. These findings highlight the importance of the XBP1-NLRP3 axis in regulating ER-mitochondrial crosstalk in IR-stressed kidneys (Fig. 6K).

Accumulating evidence suggests that the structural and functional crosstalk between the ER and mitochondria contributes to the underlying mechanism of renal IRI [16]. In our mouse model, TEM revealed that the ER from ischemia-reperfusion injured kidneys were dilated, indicating ERS. We observed that the damaged mitochondria were surrounded by abnormal ER; this implies that the mitochondria and ER collaborate in response to AKI during IRI. In addition, we observed that the expression of XBP1s, the activated form of XBP1, was higher than that of other ERS-associated molecules.

Although ER-mitochondrial crosstalk is known to play a crucial role in the kidneys, it remains unclear how the ER affects the mitochondria in IR-mediated renal injury. The NLRP3 inflammasome is induced under mitochondrial oxidative stress [28–30]. Here, consistent with previous studies [28, 31, 32], our results showed that NLRP3 inflammasome expression and activity were elevated in ischemia-reperfused kidneys, which exhibited increased clustering of NLRP3 inflammasomes on the mitochondria and the MAMs. Other studies have reported that NLRP3 is localized primarily in the ER in the resting state and only translocates to the mitochondria or MAMs under stress. In this study, however, IEM analysis revealed that NLRP3 is localized in both the mitochondria and the ER in the resting state. This discrepancy may arise from the fact that the other studies

examined immune cells, whereas we used renal tubular epithelial cells. In other words, NLRP3 subcellular localization may vary among cells.

We then examined the specific regulatory mechanisms underlying the interactions between XBP1 and NLRP3. Our lentiviral-mediated transduction experiment revealed that XBP1 overexpression promoted NLRP3 activation in TCMK-1 cells, consistent with our other finding that siRNA-mediated XBP1 downregulation reduced NLRP3 expression. Moreover, the results of our luciferase assay revealed that the expression of the spliced XBP1 isoform enhanced NLRP3 gene promoter activity. More research is essential to further elucidate these mechanisms.

XBP1 knockdown inhibited NLRP3 expression and NLRP3 inflammasome activation, thereby protecting the kidneys from ischemic reperfusion injury to some extent. This is consistent with findings from previous literature showing that the inhibition of XBP1 activity reduced NLRP3 inflammasome assembly and caspase-1 processing in a model of hepatic ischemia-reperfusion, thus reducing IRI-triggered liver injury [33, 34].

Further, Chou et al. [35] found that XBP1s deacetylation or inhibition improved cadmium-induced ERS- and NLRP3-related pyroptosis in human renal tubular epithelial cells. In general, under renal IRI in vivo and H/R in vitro, we found that XBP1 downregulation inhibited NLRP3-related inflammation and apoptosis; this protected the mitochondria by inhibiting the release of mitochondrial pro-apoptotic factors and reducing mitochondrial damage. Although our approach did not directly regulate the NLRP3 inflammasome and ROS, ROS are known to be the primary mediators of NLRP3 inflammasome activation [28, 36]. Reducing the production of mitochondrial ROS during AKI can inhibit NLRP3 inflammasome activation and reduce renal tubular epithelial cell death [37–39]. Moreover, NLRP3 inhibition via XBP1 downregulation can reduce mitochondrial damage in AKI and protect the renal tubules [40]. Apart from its role in inflammasomes, the direct or indirect inhibition of NLRP3 could also help repair tubular epithelial cells and alleviate the pathological processes of renal IRI; this is consistent with the results of our study and of other studies [41, 42]. Our results imply that NLRP3 is a potential target for clinical interventions to reduce IRI.

Based on these findings, we propose a mechanism whereby the XBP1-NLRP3 axis regulates ER-mitochondrial crosstalk in renal ischemia/reperfusion (Fig. 6K). In IRI, IRE1 α is induced, which in turn activates the splicing of XBP1 mRNA, promoting XBP1 activation. Subsequently, XBP1s becomes translocated into the nucleus to regulate the NLRP3 promoter, promoting NLRP3 expression. NLRP3 localization in the MAMs or mitochondria contributes to NLRP3-mediated inflammation and activation of apoptosis, and ROS derived from damaged mitochondria activates the NLRP3 inflammasome. Hence, the suppression of XBP1 activity may inhibit NLRP3 and its downstream pathways to prevent IRI-triggered renal injury.

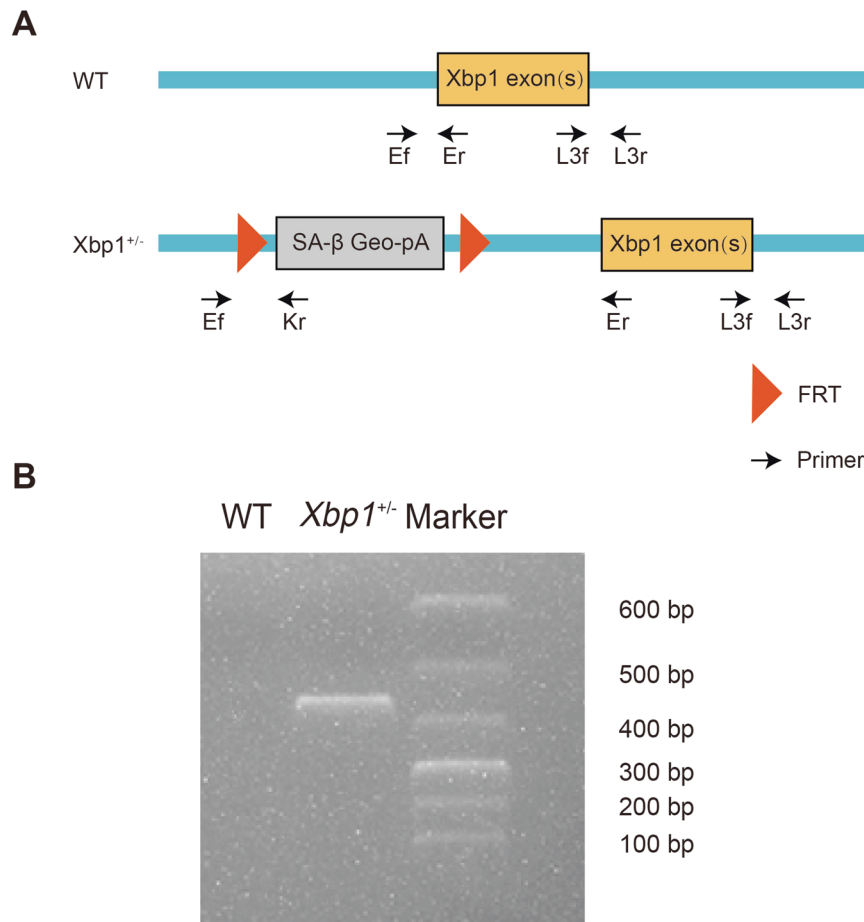


Fig. 5 Identification of $Xbp1^{+/-}$ mouse genotypes. **A** Schematic representation of the heterozygous $Xbp1^{+/-}$ mouse model. **B** Genotyping of $Xbp1^{+/-}$ mice was authenticated via PCR using Ef and Kr primers.

XBP1 has distinctive functions in different tissue types. Arthur et al. reported that XBP1 deficiency induces a pro-inflammatory response and ERS in intestinal epithelial cells, inducing apoptosis [43]. In renal tubule epithelial cells, Silvia et al. found that XBP1s overexpression contributed to renal inflammation and injury, and promoted septic AKI [44], consistent with our findings. Conversely, Claudio et al. found that XBP1 deletion in the nervous system improves the survival of mSOD1G86R transgenic mice by increasing autolysosome production and reducing apoptosis [45]. Further research is required to examine the roles of XBP1 in different tissue types and microenvironments.

These findings have important potential clinical and translational applications. In the short term, the most promising translational strategy may be to examine whether the XBP1-NLRP3 signaling pathway drives AKI in patients and whether it is a druggable target for clinical treatment. In the long term, further research is required to develop a comprehensive understanding of XBP1 as a predictive biomarker for early IR-related AKI diagnosis and as a blockade target to improve the overall survival of patients with AKI.

MATERIALS AND METHODS

Ethics approval

The study was approved by the Animal Care and Use Committee of Tongji Medical College and Nanfang Hospital, Southern Medical University. The experiments were performed in accordance with the relevant guidelines and regulations of this committee.

Mice

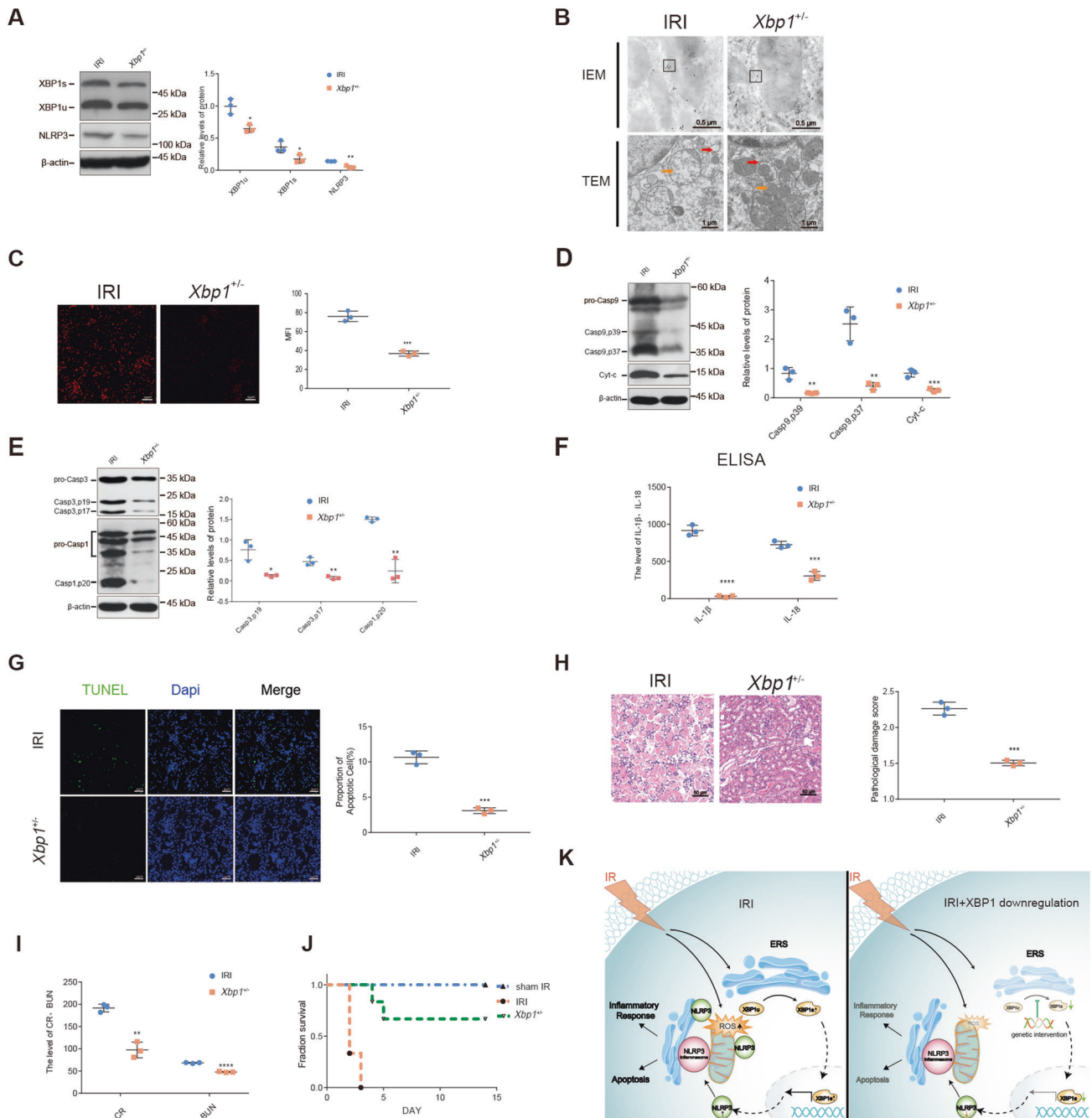
Beijing Weitong Lihua Experimental Animal Technology Co., Ltd. (China) provided the C57BL/6 mice used in this study. Heterozygous $Xbp1^{+/-}$ C57BL/6 mice (C57BL/6NTac-XBP1 < tmla<EUCOMM > Wtsi > /1cs0r1) were generated by the European Mouse Mutant Cell Repository (Phil Avner, Paris, France). All animals were raised in specific pathogen-free rooms (at 22 °C, 55% humidity, and under a 12/12 h light/dark cycle) at Tongji Hospital. The primers used to identify the mouse genotypes are listed in Supplementary Table S1.

Establishment of a renal IRI mouse model

Briefly, 8–10 week-old male mice weighing 22 ± 2 g were anesthetized via intraperitoneal injection of pentobarbital (50 mg/kg) and placed on a heating pad at 32 °C. A midline abdominal incision was made to expose the left kidney, and a noninvasive arterial clamp was used to clamp the left renal pedicle to cause renal ischemia. Afterward, the mice were placed in a constant temperature incubator at 32 °C. The vascular clamp was released after 45 min to simulate reperfusion. Meanwhile, the right kidney was removed, and the incision was sutured layer by layer. Blood and kidney samples were collected after 24 h. The control group was fed normally to observe their survival rate.

Histopathological analysis

For each slide, 10 fields of vision were randomly selected under a light microscope (at $\times 200$ magnification) to observe the shape, nuclear staining state, and lumen dilation of the renal tubular epithelial cells in each visual field. The results were graded from 0 to 3 with the following criteria: 0, no injury; 1, mild injury, presence of round epithelial cells and tubule lumen; 2, severe injury, epithelial cells flattened, nuclear staining no longer detectable, luminal dilation, and luminal hyperemia; 3, renal tubule



destruction, epithelial cells flattened, nuclear staining no longer detectable, and luminal hyperemia.

ROS detection

Renal tissue was prepared as frozen sections. An ROS staining working solution was added to the marked area, and the sections were incubated at 37 °C for 30 min, protected from light. The sections were then washed thrice with PBS on a shaker. The sections were then incubated with a DAPI solution at room temperature for 10 min to stain the nuclei. After washing, samples were observed under a fluorescence microscope (Nikon Eclipse C1, Tokyo, Japan) and photographed.

Transmission electron microscopy

Renal tissues were cut into small pieces (1 mm × 1 mm × 2 mm), fixed for at least 4 h in 2.5% glutaraldehyde at 4 °C, rinsed, and treated with 1% osmium tetroxide for 2 h. After washing, renal tissue was dehydrated using

a graded ethanol series. After penetration, embedding, and polymerization, ultrathin sections (60–80 nm) were processed using a Leica EM UC7 ultramicrotome (Leica, Wetzlar, Germany) followed by lead and uranium staining for electron microscopy (Tecnai G2 F20 TWIN; FEI Company, Hillsboro, OR).

Treatment with 4μ8C

The IRE1α inhibitor 4μ8C was purchased from MedChemExpress (CAS-number 14003-96-4; Monmouth Junction, NJ, USA), dissolved in DMSO, and added to the culture medium for 24 h (final concentration, 30 μM).

Immunoelectron microscopy

Fresh mouse renal tissue samples (1 mm³) were fixed using an IEM fixative (G124-10ML; Servicebio, Wuhan, China) overnight at 4 °C. After rinsing with pre-cooled 0.1 M phosphate buffer (PB) (3 times × 10 min each time), the tissue samples were dehydrated in a graded ethanol series.

Fig. 6 Downregulation of XBP1-NLRP3 ameliorated the crosstalk between ERS and mitochondrial damage and protected the kidneys affected by IRI in *Xbp1*^{+/-} mice. To construct the mouse IRI model, we used microvascular clips to block the left renal pedicle of the mouse for 45 min and then cut off the right kidney after opening the bloodstream. **A** Downregulation of XBP1 expression significantly suppressed the protein levels of NLRP3. Western blot; **P* < 0.05, ***P* < 0.01 vs. the IRI group (*n* = 3 samples/group per group). **B** IEM showed that the colocalization of NLRP3 and mitochondria or MAMs induced by IRI was reduced in the kidneys of *Xbp1*^{+/-} mice. Blank rectangles indicate MAMs, and the small black dots indicate the 10-nm colloidal gold particles Scale bar = 0.5 μm; ×10,000 magnification. IRI-induced ER and mitochondrial damage were significantly alleviated because of XBP1 downregulation, as shown using TEM. The red arrows indicate ER swelling, while the orange arrows indicate the damaged mitochondria. Scale bar = 1 μm; ×5000 magnification. **C** XBP1 downregulation reduced the production of ROS in the kidneys exposed to IRI, as shown via DHE staining. Scale bar = 50 μm; ×200 magnification. **D** Cleaved caspase-9 and total Cyt-c expression were reduced in the kidneys of *Xbp1*^{+/-} mice after IRI. Western blot; ***P* < 0.01, *****P* < 0.001 vs. the IRI group (*n* = 3 samples/group). **E** XBP1 downregulation alleviated NLRP3-mediated apoptosis (cleaved caspase-3 p17 and p19) and inflammation (caspase-1) in the kidneys exposed to IRI. Western blot; **P* < 0.05, ***P* < 0.01 vs. the IRI group (*n* = 3 samples/group). **F** The ELISA results indicated that the protein level of inflammatory factors IL-1β and IL-18 were decreased in the serum. *****P* < 0.001, *****P* < 0.0001 vs. the IRI group (*n* = 3 samples/group). **G** Downregulation of XBP1 expression dramatically reduced the ratio of apoptotic cells, as observed using the TUNEL assay. Scale bar = 50 μm; ×200 magnification. *****P* < 0.001 vs. the IRI group (*n* = 3 samples/group). **H** Acute renal damage was alleviated in *Xbp1*^{+/-} mice subjected to IRI, as shown using H&E staining and the pathological damage scores. Scale bar = 50 μm; ×200 magnification. *****P* < 0.001 vs. the IRI group (*n* = 3 samples/group). **I** Downregulation of XBP1 expression dramatically reduced the levels of CR and BUN in the serum. ***P* < 0.01, *****P* < 0.0001 vs. the IRI group (*n* = 3 samples/group). **J** Downregulation of XBP1 expression dramatically improved the survival of *Xbp1*^{+/-} mice. **P* < 0.05 vs. the IRI group (*n* = 3 samples/group). **K** Schematic illustration of the mechanism involving the XBP1-NLRP3 axis in regulating the ER and mitochondrial crosstalk in renal ischemia/reperfusion. IRI ischemia/reperfusion injury.

After penetration, embedding, and polymerization, ultrathin sections (70–80 nm) were processed using a Leica EM UC7 ultramicrotome and deposited on a nickel grid with a formvar film for immunolabeling. The grids prepared for immunolabeling were washed with Tris-buffered saline (TBS) droplets (room temperature; 3 times × 10 min each time) and blocked with 1% bovine serum albumin (BSA) in TBS (room temperature, 30 min). For NLRP3 single-labeling, samples were incubated with 1:50 anti-NLRP3 rabbit antibody (ab214185; Abcam, Cambridge, UK) in diluent overnight at 4 °C. The grids were returned to room temperature the next day before rinsing with TBS droplets (room temperature, for 3 × 5 min). Next, the samples were incubated with secondary antibodies conjugated with gold particles (10 nm; G7402; Sigma Aldrich, St Louis, MO), diluted in diluent (room temperature, for 20 min), incubated for 1 h at 37 °C, and finally incubated for another 30 min at room temperature. After immunolabeling, the grids were washed with TBS droplets (room temperature; 5 times × 5 min each time) and rinsed with ultrapure water (room temperature; 5 times × 5 min each time). After rinsing, the samples were stained with a saturated alcohol solution of 2% uranyl acetate in the dark for 8 min, followed by three washes in 70% ethanol and three washes in ultrapure water. After drying, the samples were observed and photographed using an HT7800 transmission electron microscope (HITACHI, Japan).

TUNEL assay

Cell death was analyzed via terminal deoxynucleotidyl transferase (TdT)-mediated dUTP digoxigenin nick-end labeling (TUNEL) in frozen kidney sections using an In Situ Cell Death Detection Kit (11684817910; Roche, Basel, Switzerland).

ELISA

Serum IL-1β and IL-18 levels were measured using commercially available ELISA kits according to their respective manufacturer's instructions (Mouse IL-18 ELISA Kit, ab216165, Abcam; Mouse IL-1β ELISA kit, DKW12-2012-096, Dakewe Biotech, China).

Cell culture and hypoxia-reoxygenation (H/R) model

The TCMK-1 cell line (CCL-139; American Type Culture Collection) was cultured in RPMI 1640 medium (Hyclone; GE Healthcare, Logan, UT, USA) supplemented with 10% fetal bovine serum (Gibco; Thermo Fisher Scientific, Waltham, MA, USA) in a 5% CO₂ atmosphere. For the hypoxia cell model, TCMK-1 cells were cultured in a pre-hypoxia serum-free medium and incubated in a tri-gas incubator (1% O₂, 5% CO₂, and 94% N₂) at 37 °C for 24 h (Don Whately Scientific, Bingley, UK). During the reoxygenation process, the spent medium was replaced with fresh complete medium, and the cells were cultured under normoxic (21% O₂) conditions for 2 h.

Immunofluorescence staining and confocal microscopy

The cells were seeded into 15 mm confocal dishes, and immunofluorescence staining was performed after the intervention. MitoTracker Red

CMXRos (Life Technologies, Carlsbad, CA, USA), diluted in serum-free medium to 100 nM, was added to the cells, which were then incubated in the dark at 37 °C for 30 min. ER Tracker Blue White DPX dye (Life Technologies, Carlsbad, CA, USA), diluted in serum-free medium to a final concentration of 200 nM, was then added to the cells, which were incubated in the dark at 37 °C for 30 min. Next, the cells were fixed with 4% paraformaldehyde for 15 min and permeabilized using 0.3% after washing three times with PBS. Triton for 15 min, and sealed with 5% BSA for 30 min. Primary antibodies (1:100) were added. The cells were incubated in the dark at 4 °C overnight. DyLight 488 goat anti-rabbit IgG (1:200; A23220; Abbkine, Wuhan, China) was then added, and the cells were incubated in the dark at 37 °C for 1 h. Images were captured using a TIE confocal microscope (Nikon, Tokyo, Japan). A plot profile was generated using ImageJ software to assess the degree of colocalization.

XBP1 siRNA knockdown and overexpression

Lentivirus-overexpressing XBP1 particles were purchased from Hanbio Biotechnology Co., Ltd. (Shanghai, China). TCMK-1 cells were seeded at a density of 2 × 10⁵ cells/well in six-well plates 12 h before transfection. siRNA transfection was performed using Lipofectamine 2000 (Invitrogen; Thermo Fisher Scientific, Inc., Waltham, MA, USA), and treatments were performed 24 h after transfection. The lentiviral solution (1 × 10⁹ TU/mL) was added to the culture medium (40 μL/well, 4 × 10⁷ TU) at a 50% multiplicity of infection. After 24 h, the spent medium was replaced and the cells were cultured for another 24 h. Stable XBP1-overexpressing strains were screened using a culture medium containing 3 μg/mL puromycin. The siRNA sequences used in this study can be found in Supplementary Table S2.

Western blotting

Protein quantification was performed using ImageJ software. The antibodies used are listed in Supplementary Table S3.

Flow cytometry

TCMK-1 cells were cultured in six-well plates and harvested using trypsin without EDTA before and after staining. Cellular ROS, mitochondrial ROS, apoptosis, and MMP were determined using a Reactive Oxygen Species Assay kit (Beyotime Institute of Biotechnology, Shanghai, China), MitoSOX kit (Life Technologies, Carlsbad, CA, USA), Annexin V-PI staining kit, and JC-1 detection kit (Beyotime Institute of Biotechnology, Shanghai, China), respectively. The cells were then stained according to the respective manufacturer's instructions and analyzed via flow cytometry. Ten thousand events were recorded using the FACSCalibur system (BD Biosciences, CA, USA), and the resulting data were analyzed using FlowJo software.

Real-time quantitative reverse-transcription PCR

Total cell RNA was extracted, and PCR was conducted using the appropriate reaction systems. The total RNA obtained was reverse-transcribed into cDNA (15 min at 37 °C, 5 s at 85 °C, indefinite hold at 4 °C). The obtained

cDNA stock solution was diluted to 1/8 of its original concentration and amplified according to the instructions of the real-time quantitative PCR MIX kit. The reaction solution was subjected to the following conditions: pre-denaturation at 94 °C for 30 s, then 40 cycles at 94 °C for 5 s and 60 °C for 30 s. The relative mRNA expression levels were then analyzed using β -actin as the internal reference gene. The primer sequences used in this experiment can be found in Supplementary Table S4.

Dual-luciferase assay

Healthy 293T cells were seeded in 24-well culture plates one day before plasmid transfection. All cell transfection experiments were performed using X-tremeGENE HP DNA Transfection Reagent (Roche, Basel, Switzerland). The expression of fluorescently labeled genes was observed under a fluorescence microscope 48 h after transfection. Luciferase expression was then evaluated using a Dual-Luciferase Reporter Assay System (Promega, Madison, WI). Information about the plasmids and treatment groups can be found in Supplementary Table S5.

Statistical analysis

All analyses were performed using GraphPad Prism 8 software (La Jolla, CA). Normally distributed data were expressed as the mean \pm standard error of the mean. Survival data were compared using the log-rank test. Comparisons among groups were performed using a *t*-test (between two groups) or ANOVA (among more than two groups).

DATA AVAILABILITY

Full images of western blotting had been included in Supplementary Materials. Other data are available from the corresponding authors for reasonable grounds.

REFERENCES

- Li PK, Burdman EA, Mehta RL. Acute kidney injury: global health alert. *Kidney Int.* 2013;83:372–6.
- Ronco C, Bellomo R, Kellum JA. Acute kidney injury. *Lancet.* 2019;394:1949–64.
- Devarajan P. Update on mechanisms of ischemic acute kidney injury. *J Am Soc Nephrol.* 2006;17:1503–20.
- Bonventre JV, Yang L. Cellular pathophysiology of ischemic acute kidney injury. *J Clin Invest.* 2011;121:4210–21.
- Mahfoudh-Boussaid A, Zaouali MA, Hauet T, Hadj-Ayed K, Miled AH, Ghoul-Mazgar S, et al. Attenuation of endoplasmic reticulum stress and mitochondrial injury in kidney with ischemic postconditioning application and trimetazidine treatment. *J Biomed Sci.* 2012;19:71.
- Maekawa H, Inagi R. Pathophysiological role of organelle stress/crosstalk in aki-to-ckd transition. *Semin Nephrol.* 2019;39:581–8.
- Yoshida H, Haze K, Yanagi H, Yura T, Mori K. Identification of the cis-acting endoplasmic reticulum stress response element responsible for transcriptional induction of mammalian glucose-regulated proteins. Involvement of basic leucine zipper transcription factors. *J Biol Chem.* 1998;273:33741–9.
- Tirasophon W, Welihinda AA, Kaufman RJ. A stress response pathway from the endoplasmic reticulum to the nucleus requires a novel bifunctional protein kinase/endoribonuclease (ire1p) in mammalian cells. *Genes Dev.* 1998;12:1812–24.
- Harding HP, Zhang Y, Ron D. Protein translation and folding are coupled by an endoplasmic-reticulum-resident kinase. *Nature.* 1999;397:271–4.
- Prachasilchai W, Sonoda H, Yokota-Ikeda N, Oshikawa S, Aikawa C, Uchida K, et al. A protective role of unfolded protein response in mouse ischemic acute kidney injury. *Eur J Pharmacol.* 2008;592:138–45.
- Malhotra JD, Kaufman RJ. Endoplasmic reticulum stress and oxidative stress: a vicious cycle or a double-edged sword? *Antioxid Redox Signal.* 2007;9:2277–93.
- Yan M, Shu S, Guo C, Tang C, Dong Z. Endoplasmic reticulum stress in ischemic and nephrotoxic acute kidney injury. *Ann Med.* 2018;50:381–90.
- Deniaud A, Sharaf EDO, Maillier E, Poncet D, Kroemer G, Lemaire C, et al. Endoplasmic reticulum stress induces calcium-dependent permeability transition, mitochondrial outer membrane permeabilization and apoptosis. *Oncogene.* 2008;27:285–99.
- Chander V, Chopra K. Protective effect of nitric oxide pathway in resveratrol renal ischemia-reperfusion injury in rats. *Arch Med Res.* 2006;37:19–26.
- Swanson KV, Deng M, Ting JP. The nlrp3 inflammasome: molecular activation and regulation to therapeutics. *Nat Rev Immunol.* 2019;19:477–89.
- Inoue T, Maekawa H, Inagi R. Organelle crosstalk in the kidney. *Kidney Int.* 2019;95:1318–25.
- Hayashi T, Su TP. Sigma-1 receptor chaperones at the er-mitochondrion interface regulate ca(2+) signaling and cell survival. *Cell.* 2007;131:596–610.
- Higo T, Hamada K, Hisatsune C, Nukina N, Hashikawa T, Hattori M, et al. Mechanism of er stress-induced brain damage by ip(3) receptor. *Neuron.* 2010;68:865–78.
- Hammadi M, Oulidi A, Gackière F, Katsogiannou M, Slomianny C, Roudbaraki M, et al. Modulation of er stress and apoptosis by endoplasmic reticulum calcium leak via translocon during unfolded protein response: involvement of grp78. *FASEB J.* 2013;27:1600–9.
- Roderick HL, Lechleiter JD, Camacho P. Cytosolic phosphorylation of calnexin controls intracellular ca(2+) oscillations via an interaction with serca2b. *J Cell Biol.* 2000;149:1235–48.
- Carreras-Sureda A, Jaña F, Urrea H, Durand S, Mortenson DE, Sagredo A, et al. Non-canonical function of ire1 α determines mitochondria-associated endoplasmic reticulum composition to control calcium transfer and bioenergetics. *Nat Cell Biol.* 2019;21:755–67.
- Takeda K, Nagashima S, Shiiba I, Uda A, Tokuyama T, Ito N, et al. Mitol prevents er stress-induced apoptosis by ire1 α ubiquitylation at er-mitochondria contact sites. *EMBO J.* 2019;38:e100999.
- Verfaillie T, Rubio N, Garg AD, Bultynck G, Rizzuto R, Decuypere JP, et al. Perk is required at the er-mitochondrial contact sites to convey apoptosis after ros-based er stress. *Cell Death Differ.* 2012;19:1880–91.
- Iwasawa R, Mahul-Mellier AL, Datler C, Pazarentzos E, Grimm S. Fis1 and bap31 bridge the mitochondria-er interface to establish a platform for apoptosis induction. *EMBO J.* 2011;30:556–68.
- Kriss CL, Pinilla-Ibarz JA, Mailloux AW, Powers JJ, Tang CH, Kang CW, et al. Overexpression of tcl1 activates the endoplasmic reticulum stress response: a novel mechanism of leukemic progression in mice. *Blood.* 2012;120:1027–38.
- Lee AH, Iwakoshi NN, Glimcher LH. Xbp-1 regulates a subset of endoplasmic reticulum resident chaperone genes in the unfolded protein response. *Mol Cell Biol.* 2003;23:7448–59.
- Zhang J, Zhang J, Ni H, Wang Y, Katwal G, Zhao Y, et al. Downregulation of xbp1 protects kidney against ischemia-reperfusion injury via suppressing hrd1-mediated rnf2 ubiquitylation. *Cell Death Discov.* 2021;7:44.
- Zhou R, Yazdi AS, Menu P, Tschopp J. A role for mitochondria in nlrp3 inflammasome activation. *Nature.* 2011;469:221–5.
- Wen Y, Liu YR, Tang TT, Pan MM, Xu SC, Ma KL, et al. Mros-txnip axis activates nlrp3 inflammasome to mediate renal injury during ischemic aki. *Int J Biochem Cell Biol.* 2018;98:43–53.
- He W, Ye S, Zeng C, Xue S, Hu X, Zhang X, et al. Hypothermic oxygenated perfusion (hope) attenuates ischemia/reperfusion injury in the liver through inhibition of the txnip/nlrp3 inflammasome pathway in a rat model of donation after cardiac death. *FASEB J.* 2018;32:6212–27.
- Bronner DN, Abuaita BH, Chen X, Fitzgerald KA, Nuñez G, He Y, et al. Endoplasmic reticulum stress activates the inflammasome via nlrp3- and caspase-2-driven mitochondrial damage. *Immunity.* 2015;43:451–62.
- Subramanian N, Natarajan K, Clatworthy MR, Wang Z, Germain RN. The adaptor mavs promotes nlrp3 mitochondrial localization and inflammasome activation. *Cell.* 2013;153:348–61.
- Li C, Jin Y, Wei S, Sun Y, Jiang L, Zhu Q, et al. Hippo signaling controls nlr family pyrin domain containing 3 activation and governs immunoregulation of mesenchymal stem cells in mouse liver injury. *Hepatology.* 2019;70:1714–31.
- Yue S, Zhu J, Zhang M, Li C, Zhou X, Zhou M, et al. The myeloid heat shock transcription factor 1/ β -catenin axis regulates nlr family, pyrin domain-containing 3 inflammasome activation in mouse liver ischemia/reperfusion injury. *Hepatology.* 2016;64:1683–98.
- Chou X, Ding F, Zhang X, Ding X, Gao H, Wu Q. Sirtuin-1 ameliorates cadmium-induced endoplasmic reticulum stress and pyroptosis through xbp-1s deacetylation in human renal tubular epithelial cells. *Arch Toxicol.* 2019;93:965–86.
- Hou Y, Wang Q, Han B, Chen Y, Qiao X, Wang L. Cd36 promotes nlrp3 inflammasome activation via the mtros pathway in renal tubular epithelial cells of diabetic kidneys. *Cell Death Dis.* 2021;12:523.
- Lin Q, Li S, Jiang N, Shao X, Zhang M, Jin H, et al. Pink1-parkin pathway of mitophagy protects against contrast-induced acute kidney injury via decreasing mitochondrial ros and nlrp3 inflammasome activation. *Redox Biol.* 2019;26:101254.
- Pi S, Nie G, Wei Z, Yang F, Wang C, Xing C, et al. Inhibition of ros/nlrp3/caspase-1 mediated pyroptosis alleviates excess molybdenum-induced apoptosis in duck renal tubular epithelial cells. *Ecotoxicol Environ Saf.* 2021;208:111528.
- Yang SK, Han YC, He JR, Yang M, Zhang W, Zhan M, et al. Mitochondria targeted peptide ss-31 prevent on cisplatin-induced acute kidney injury via regulating mitochondrial ros-nlrp3 pathway. *Biomed Pharmacother.* 2020;130:110521.
- Song SJ, Kim SM, Lee SH, Moon JY, Hwang HS, Kim JS, et al. Rhabdomyolysis-induced aki was ameliorated in nlrp3 ko mice via alleviation of mitochondrial lipid peroxidation in renal tubular cells. *Int J Mol Sci.* 2020;21:8564.
- Bakker PJ, Butter LM, Claessen N, Teske GJ, Sutterwala FS, Florquin S, et al. A tissue-specific role for nlrp3 in tubular epithelial repair after renal ischemia/reperfusion. *Am J Pathol.* 2014;184:2013–22.

42. Kim HJ, Lee DW, Ravichandran K, Keys DO, Akcay A, Nguyen Q, et al. Nlrp3 inflammasome knockout mice are protected against ischemic but not cisplatin-induced acute kidney injury. *J Pharmacol Exp Ther.* 2013;346:465–72.
43. Kaser A, Lee AH, Franke A, Glickman JN, Zeissig S, Tilg H, et al. Xbp1 links er stress to intestinal inflammation and confers genetic risk for human inflammatory bowel disease. *Cell.* 2008;134:743–56.
44. Ferrè S, Deng Y, Huen SC, Lu CY, Scherer PE, Igarashi P, et al. Renal tubular cell spliced x-box binding protein 1 (xbp1s) has a unique role in sepsis-induced acute kidney injury and inflammation. *Kidney Int.* 2019;96:1359–73.
45. Hetz C, Thielen P, Matus S, Nassif M, Court F, Kiffin R, et al. Xbp-1 deficiency in the nervous system protects against amyotrophic lateral sclerosis by increasing autophagy. *Genes Dev.* 2009;23:2294–306.

ACKNOWLEDGEMENTS

This study was funded by National Natural Science Foundation of China (Grant No. 82270784, 82070770, 82170772, 81873623, 81570678, 81500573), Guangdong Basic and Applied Basic Research Foundation (Grant No. 2023A1515012276) and Academician Shusen Lanjuan Talent Foundation (grant to Yuchen Wang).

AUTHOR CONTRIBUTIONS

HN, YM, and NG designed and directed the study. HN, YW, and YL wrote the manuscript. HN, ZO, YW, YL, KS, JZ, JSZ, WD, WZ, RX, and JX performed experimental work and analyzed the data. HN, YW, NG, and YM revised the manuscript.

COMPETING INTERESTS

The authors declare no competing interests.

ADDITIONAL INFORMATION

Supplementary information The online version contains supplementary material available at <https://doi.org/10.1038/s41420-023-01360-x>.

Correspondence and requests for materials should be addressed to Nianqiao Gong or Yun Miao.

Reprints and permission information is available at <http://www.nature.com/reprints>

Publisher's note Springer Nature remains neutral with regard to jurisdictional claims in published maps and institutional affiliations.



Open Access This article is licensed under a Creative Commons Attribution 4.0 International License, which permits use, sharing, adaptation, distribution and reproduction in any medium or format, as long as you give appropriate credit to the original author(s) and the source, provide a link to the Creative Commons license, and indicate if changes were made. The images or other third party material in this article are included in the article's Creative Commons license, unless indicated otherwise in a credit line to the material. If material is not included in the article's Creative Commons license and your intended use is not permitted by statutory regulation or exceeds the permitted use, you will need to obtain permission directly from the copyright holder. To view a copy of this license, visit <http://creativecommons.org/licenses/by/4.0/>.

© The Author(s) 2023